Stratospheric Influence on Tropopause Height: The Radiative Constraint

JOHN THUBURN

Department of Meteorology, University of Reading, Reading, United Kingdom

GEORGE C. CRAIG

Joint Centre for Mesoscale Meteorology, Department of Meteorology, University of Reading, Reading, United Kingdom

(Manuscript received 27 July 1998, in final form 23 March 1999)

ABSTRACT

Earlier theoretical and modeling work introduced the concept of a radiative constraint relating tropopause height to tropospheric lapse rate and other factors such as surface temperature. Here a minimal quantitative model for the radiative constraint is presented and used to illustrate the essential physics underlying the radiative constraint, which involves the approximate balance between absorption and emission of thermal infrared (IR) radiation determining tropopause temperature.

The results of the minimal model are then extended in two ways. First, the effects of including a more realistic treatment of IR radiation are quantified. Second, the radiative constraint model is extended to take into account non-IR warming processes such as solar heating and dynamical warming near the tropopause. The sensitivity of tropopause height to non-IR warming is estimated to be a few kilometers per K day^{-1}, with positive warming leading to a lower tropopause. Sensitivities comparable to this are found in GCM experiments in which imposed changes in the ozone distribution or in the driving of the stratospheric residual mean meridional circulation lead to changes in tropopause height. In the Tropics the influence of the stratospheric circulation is found to extend down at least as far as the main convective outflow level, some 5 km below the temperature minimum.

1. Introduction

The tropopause has been defined in a variety of ways, all of which are, to some extent, empirical. Examples include definitions in terms of temperature lapse rate (e.g., Lewis 1991), potential vorticity (e.g., Hoerling et al. 1991), or chemical composition (e.g., Bethan et al. 1996). These definitions are necessarily empirical because we do not yet have an adequate understanding of the fundamental physical nature of the tropopause that could provide a physically based definition. One suggestion for a physically based definition of the tropopause is that it separates two regions, the stratosphere and the troposphere, with qualitatively different heat budgets. The simplest version of this idea has the stratosphere in or close to radiative equilibrium while the tropospheric heat budget is dominated by convection in the Tropics or eddy heat transport in the extratropics. This idea is implicit in the radiative constraint on tropopause height proposed by Held (1982) and further discussed by Thuburn and Craig (1997). The idea also arises in attempting to quantify radiative forcing of climate change; Forster et al. (1997) show that in a radiative–convective model the radiative forcing of the surface–troposphere system, as defined by IPCC (1994), is sensitive to the definition of the tropopause used, and they suggest that the most appropriate definition is the boundary between the convectively adjusted region and the radiative equilibrium region above. Note, by the way, that in radiative–convective models the tropopause defined in this way can be several kilometers below the level of minimum temperature (e.g., Sinha and Shine 1994). In this paper we pursue further the idea that the defining property of the tropopause is that it separates two regions with qualitatively different heat budgets; we refine the concept of a radiative constraint on tropopause height and examine some of its implications.

The key physical assumption underlying the concept of a radiative constraint is that the tropopause and lowermost stratosphere are close to radiative equilibrium in the infrared (IR) bands. This assumption leads to a relationship, expected to be valid on timescales of a few weeks or longer, between tropopause height H, surface temperature T_*, and tropospheric lapse rate γ (and other quantities including the optical depth profile τ). Thuburn and Craig (1997), following and extending the work of Held (1982), used a simple, two-stream, gray

Corresponding author address: Dr. John Thuburn, Department of Meteorology, University of Reading, Earley Gate, P.O. Box 243, Reading RG6 6BB, United Kingdom.
E-mail: swsthubn@met.rdg.ac.uk

atmosphere model for IR radiation to express the radiative constraint quantitatively. This simple model predicts that H should increase significantly as γ decreases. Also, when the τ profile is parameterized in terms of γ and T_* to account for variations of atmospheric moisture with temperature, the simple model predicts a strong sensitivity of tropopause height to T_*. The predictions of this simple model of the radiative constraint agreed quite well, at least in the extratropics, with global circulation model (GCM) experiments in which the tropopause height varied in response to imposed changes in surface temperature.

The agreement is perhaps surprising, given that several factors have been neglected in the simple model. These include solar heating in the stratosphere, dynamical warming in the stratosphere, clouds, the effects of CO_2 and O_3 on IR, variations in relative humidity, and the spectral dependence of the radiative properties of water vapor. The possible importance of these neglected factors is yet to be quantified. For example, solar heating rates and dynamical warming rates are both typically a fraction of a degree per day in the lower stratosphere. These are significantly smaller than typical tropospheric heating rates due to convection, for example, but it is not immediately obvious what constitutes ''small'' in the context of the radiative constraint, and what is small enough to be negligible.

In this paper we reassess our simple model for the radiative constraint and investigate the possible importance of some of the neglected factors mentioned above. In section 2 we review the simple model and isolate the most essential physics underlying it. In section 3 we discuss the possible importance of the effects of CO_2, O_3, and the spectral dependence of the radiative properties of water vapor. In section 4 we show that solar heating and dynamical warming (i.e., non-IR warming) in the lower stratosphere can be included in our radiative constraint model in a straightforward way by regarding them as part of the specified forcing, like the surface temperature, rather than part of the response, like the IR radiation. We show that the relative importance of non-IR warming, in particular whether it can be regarded as small, can be measured by comparison with the heating by absorption of upwelling IR. We estimate the sensitivity of tropopause height to non-IR warming in the lower stratosphere and find that typical dynamical warming rates can have a significant effect on tropopause height. This sensitivity is confirmed in GCM experiments (section 5) in which ozone heating is modified or imposed forces in the stratosphere are used to modify the residual mean meridional circulation and dynamical warming.

2. Review of the simple radiative constraint model, and a further simplification

The version of the radiative constraint examined by Thuburn and Craig (1997) is based on the two-stream gray atmosphere IR radiative transfer model of Goody (1964). Solar radiation is neglected in the first instance. Let $\tau(z)$ be the optical depth measured from the top of the atmosphere; let $U(\tau)$ and $D(\tau)$ be the upward and downward IR irradiances; $B(\tau) = \sigma T(\tau)^4$ where $\sigma = 5.67 \times 10^{-8}$ W m^{-2} K^{-4} is the Stephan–Boltzmann constant; and $T(\tau)$ is the temperature. Then the profiles of U and D are modeled using the equations

$$\frac{dU}{d\tau} = \frac{3}{2}(U - B) \tag{1}$$

$$\frac{dD}{d\tau} = \frac{3}{2}(B - D), \tag{2}$$

with boundary conditions $U = \sigma T_*^4$ at $z = 0$ and $D = 0$ at $\tau = 0$.

If we assume that the stratosphere is in radiative equilibrium in the IR—that is, that $d(U - D)/d\tau = 0$ there—then (1) and (2) imply that $2B = U + D$ there. It is then easy to show that in the stratosphere $(U, D, B) = (1 + 3\tau/4, 3\tau/4, 1/2 + 3\tau/4)I$, where I is the as yet undetermined outgoing longwave radiation (OLR) $U(\tau = 0)$. The problem then is to find the height H_{RAD} that allows the specified tropospheric temperature profile $T = T_* - \gamma z$ for $z < H_{\mathrm{RAD}}$ to be matched to this stratospheric radiative equilibrium solution for $z > H_{\mathrm{RAD}}$. The solution can be found, given T_* and γ and the vertical profile of τ, by numerically integrating (1) up from the lower boundary to the level $z = H_{\mathrm{RAD}}$ at which the ratio U/B first attains the value $(1 + 3\tau/4)/(1/2 + 3\tau/4)$ required for radiative equilibrium.

One of the assumptions underlying this model is that the temperature profile is continuous at the tropopause. This is consistent with the radiative models (1) and (2), which would damp any temperature discontinuity provided that the τ profile is sufficiently smooth. This is in addition to any convective adjustment that might occur if T decreased too rapidly with height.

This already simple model can be further simplified, with virtually no change to the calculated results for realistic parameters, in a way that highlights the essential physics underlying the radiative constraint. With the exception of the 15-μm CO_2 band (to be discussed in the next section), the stratosphere and upper troposphere are optically thin in the IR. This implies that the upwelling irradiance at the tropopause is given, to a first approximation, by integrating over the lowest, optically thick, part of the troposphere. It also implies that, to a first approximation, the absorption of downwelling irradiance at the tropopause can be neglected, and hence that $2B \approx U$ for radiative equilibrium at the tropopause and in the stratosphere. Thus, the temperature and radiative properties of the lowest part of the troposphere determine the upwelling irradiance at the tropopause, and the balance between absorption and emission at the tropopause determines B there, and hence the tropopause temperature T_{TP}. This is the essential physics underlying the radiative constraint. Once T_{TP} is known, the

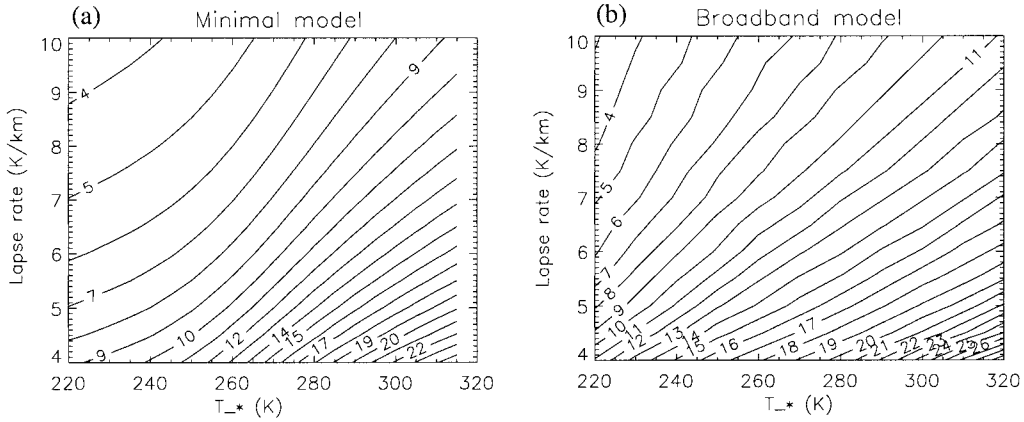

FIG. 1. (a) Tropopause height (km) as a function of surface temperature and tropospheric lapse rate, predicted by the minimal radiative constraint model. (b) As in (a), but for the broadband radiative–convective model.

tropopause height is easily determined from the tropospheric temperature profile:

$$H_{\mathrm{RAD}} = (T_* - T_{\mathrm{TP}})/\gamma. \tag{3}$$

We will refer to this as our minimal model for the radiative constraint.

It is useful to note how the radiative constraint model is related to radiative–convective models. In fact, the radiative constraint model is essentially a radiative–convective model, though with a slightly different interpretation: we make no assumption about what determines the tropospheric lapse rate γ or what value γ takes; it is left as a free parameter in the problem, and the sensitivity of H_{RAD} to γ is predicted by the model. Also, radiative–convective models are often considered to represent a global horizontal average atmosphere (e.g., Goody 1964). Then, on long enough timescales the OLR must balance the incoming solar radiation, and this requirement determines the stratospheric temperature profile independently of what happens below the tropopause (at least for a gray atmosphere) and allows the global mean surface temperature T_* to be deduced. In contrast, the radiative constraint is assumed to operate in individual atmospheric columns or latitude bands on timescales of a few weeks. Then there is no requirement for OLR to balance incoming solar radiation locally, and it is more appropriate to take specified T_* because T_* is influenced by other, longer timescale, processes such as the ocean circulation.

Figure 1a shows $H_{\mathrm{RAD}}(T_*, \gamma)$ calculated using the minimal model. The optical depth profile used in this calculation was parameterized in terms of T_* and γ as

$$\tau(z) = \tau_* e^{-z/z_0}, \tag{4}$$

where

$$\tau_* = 0.2 w_* z_0 \quad \text{and} \tag{5}$$

$$z_0 = 1/(0.07\gamma). \tag{6}$$

Here w_*, the water vapor saturation mixing ratio at the ground, is given by

$$w_* = \frac{1}{p_0} 380.03 \exp\left\{\frac{17.260(T_* - 273.16)}{(T_* - 35.86)}\right\} \tag{7}$$

(Lowe 1977), where $p_0 = 10^5$ Pa. This parameterized profile represents the effects of a distribution of water vapor, the dominant radiatively active gas in the IR, with roughly constant relative humidity. The coefficient 0.2 in (5) was chosen to give a global mean value of τ_* close to the value 4.0 suggested by Goody (1964) and used by Held (1982).

Note that this value 0.2 of the coefficient in (5) is different from the value 0.05 used by Thuburn and Craig (1997). Thuburn and Craig arrived at the value 0.05 by tuning to obtain good agreement between their simple model of the radiative constraint and a control GCM integration; however, that tuning used an incorrect estimate for the mean tropospheric lapse rate $[g/C_{\mathrm{p}} + (\theta_* - \theta(H))/H$ rather than $(T_* - T(H))/H]$. When the correct estimate of tropospheric lapse rate is used the agreement between the simple radiative constraint model and the control GCM integration is improved by using the larger value 0.2.

According to Fig. 1a, our minimal model predicts that H should increase both as T_* increases and as γ decreases. In the lower right half of the figure the sensitivity to T_* is quite strong. This occurs through the strong dependence of water vapor concentration on temperature. In the upper left half of the figure the sensitivity to T_* is weaker. This is because those parameter values imply cold tropospheric temperatures and low water vapor concentrations leading to an optically thin atmosphere in our minimal model, so that upwelling IR radiation emitted at the ground becomes increasingly important in controlling tropopause temperature. In fact an analytic solution can be found in the limiting case in which the whole atmosphere is optically thin. The upwelling irradiance at the tropopause is then approximately equal to its value at the surface, $U \approx \sigma T_*^4$, implying $T_{\mathrm{TP}} \approx (1/2)^{1/4} T_*$ and $H_{\mathrm{RAD}} \approx (1 - (1/2)^{1/4}) T_*/\gamma \approx 0.159 T_*/\gamma$. However, this limit applies only for ex-

tremely cold surface temperatures, $T_* < 240$ K, for which, as shown in the next section, the gray atmosphere model becomes inaccurate.

3. Spectral dependence of IR radiation

Our minimal model for the radiative constraint is based on a gray atmosphere model for IR radiation; that is, the optical depth profile is assumed to be independent of wavelength. However, the real atmosphere has optical properties that depend strongly on wavelength. In particular, there are strong absorption–emission bands at around 15-μm due to CO_2 and around 9.6-μm due to O_3, and an otherwise relatively transparent window region between about 8 and 12-μm. In this section we use a broadband radiative transfer model to estimate the impact of the gray atmosphere approximation for the radiative constraint. The broadband model used is a version of the Morcrette (1990) scheme, further developed by Zhong and Haigh (1995) and Zhong et al. (1996). It includes six IR bands accounting for water vapor lines and continuum, CO_2, and O_3. Clouds were not included in any of our calculations.

First we used the broadband model to check the magnitude of the downwelling irradiance near the tropopause, which is neglected in our minimal model. Calculations using typical temperature and constituent profiles for a range of latitudes gave downwelling IR irradiances at the tropopause of 10–30 W m^{-2}. These are certainly much smaller than the calculated upwelling IR irradiances, which were in the range 200–300 W m^{-2}. Moreover, further calculations without the effects of CO_2 confirmed that much of this downwelling, typically 10 W m^{-2}, occurs in the 15-μm CO_2 band associated with emission by CO_2 in the stratosphere. We will argue below that radiation in the 15-μm CO_2 band has little effect on the tropopause temperature, so that the effect of the downwelling irradiance at the tropopause is even smaller than suggested by the above figure of 10–30 W m^{-2}.

To investigate the importance of spectral variations in optical properties for the radiative constraint we used the broadband radiation model to construct a radiative–convective model. The surface temperature T_* and the tropospheric lapse rate γ are specified. A constant CO_2 mixing ratio of 456 ppmv and an O_3 profile typical of the Tropics are used. An arbitrary initial temperature profile is chosen, and from this a water vapor profile is calculated to give a relative humidity of 50%, subject to the constraint that water vapor mixing ratio may not increase with altitude. The model is then stepped forward in time, as follows, until an equilibrium solution is attained: first, the radiative heating rates are calculated and used to modify the temperature; then, at any level where $T < T_* - \gamma z$, T is adjusted to equal $T_* - \gamma z$; and finally, the 50% relative humidity water vapor profile is recalculated. When the equilibrium solution is attained, the top of the adjusted region is identified as the radiative constraint tropopause $H_{\rm RAD}$. The radiation calculations omit the effects of solar radiation and clouds, so that this radiative–convective model is as similar as possible to the simple model described in section 2, except for the extra detail in IR radiation calculation.

Figure 1b shows $H_{\rm RAD}(T_*, \gamma)$ calculated using the broadband radiative–convective model for comparison with the results of the minimal model shown in Fig. 1a. Over the most practically relevant parameter range, $T_* \approx 260$–300 K, $\gamma \approx 5$–7 K km^{-1}, $H_{\rm RAD}$ from the broadband model is 2–3km higher than $H_{\rm RAD}$ from the minimal model. However, for the same parameter range, the sensitivity of $H_{\rm RAD}$ to T_* and γ is very similar for the two models. An interesting feature of Fig. 1b, in contrast to Fig. 1a, is that the broadband model retains a strong sensitivity of $H_{\rm RAD}$, to T_* even for cold surface temperatures and steep lapse rates.

It is possible to argue on theoretical grounds that both the 15-μm CO_2 band and the 9.6-μm O_3 band should have a only a small effect on the balance between absorption and emission that determines tropopause temperature, that is, on the radiative constraint. The broadband model allows this prediction to be checked empirically.

The 15-μm CO_2 band is optically thick up to the altitude of the lower stratosphere. This implies that as we move away from the lower boundary, absorption and emission quickly come into equilibrium, so there is very little net heating due to radiation in the 15-μm CO_2 band, irrespective of the value of temperature provided that it has no very large vertical gradients. This was confirmed by calculating heating rate profiles using the broadband radiative transfer model for a range of latitudes both with and without the effects of CO_2. Removing CO_2 had a significant effect on the IR heating rate in the lower troposphere below about 400 hPa and in the stratosphere above about 70 hPa but a small effect, less than about 0.1 K day^{-1}, on tropopause heating rates. The importance of this amount of CO_2 heating can be estimated as follows. Assume that at the tropopause the CO_2 heating is in equilibrium with the rest of the IR heating, so that

$$0 = \rho C_p \dot{T}_{\rm CO_2} + \frac{d}{dz}(U' - D') = \rho C_p \dot{T}_{\rm CO_2} + \frac{3}{2}(U' - 2B')\frac{d}{dz}\tau', \tag{8}$$

where a prime indicates a quantity in the non-CO_2 part of the spectrum, and we have neglected absorption of downwelling radiation. Rearranging for B' gives

$$B' = \frac{1}{2}U' + \frac{1}{3}\frac{dz}{d\tau'}\rho C_p \dot{T}_{\rm CO_2}. \tag{9}$$

Thus, a small heating from the optically thick 15-μm CO_2 band will have a small effect on B' and the tro-

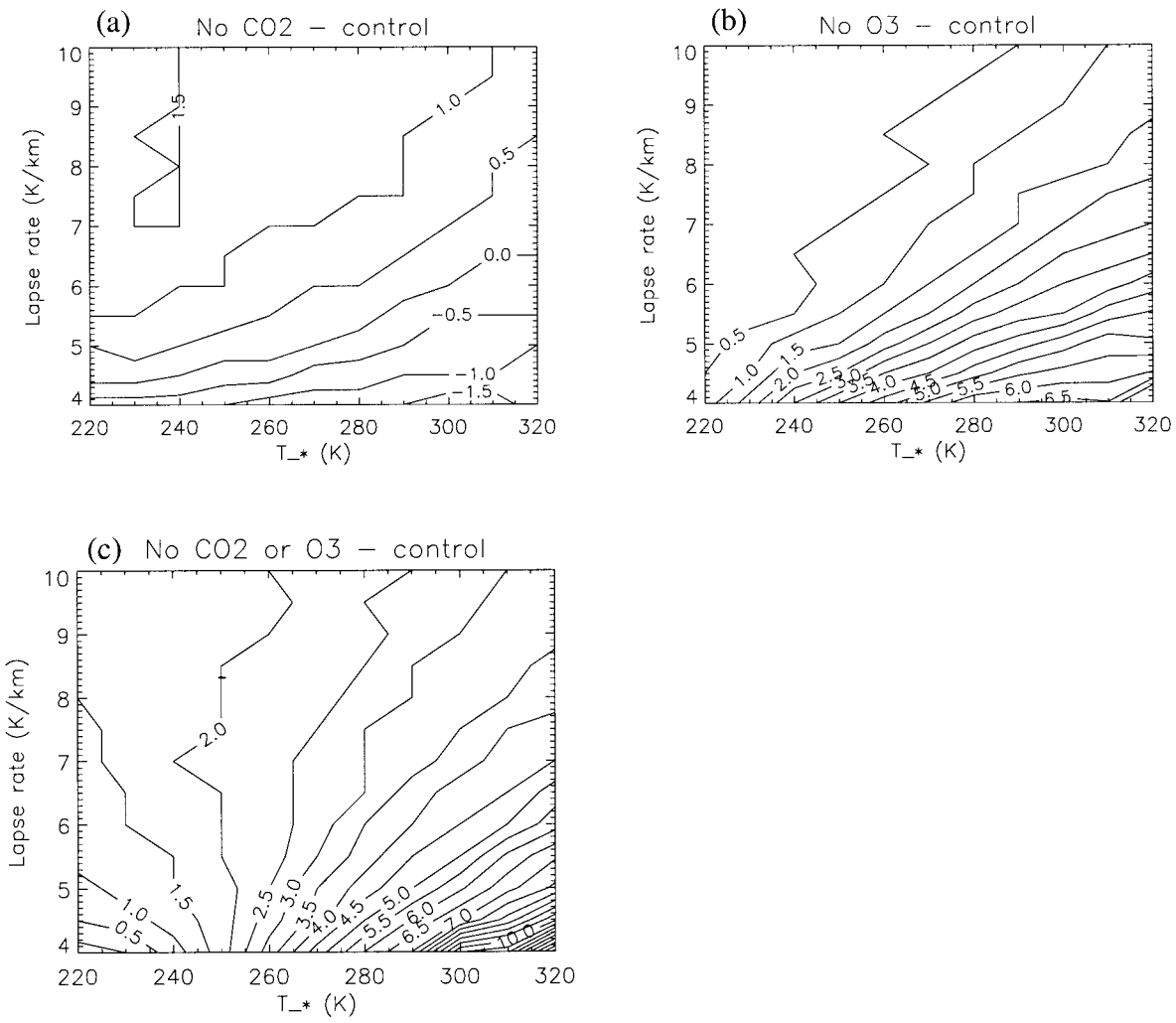

FIG. 2. (a) Change in tropopause height (km) resulting from suppressing the effects of CO_2 in the broadband radiative–convective model. (b) Change in tropopause height (km) resulting from suppressing the IR effects of O_3. (c) Change in tropopause height (km) resulting from suppressing the effects of both CO_2 and O_3.

popause temperature, except when the non-CO_2 part of the spectrum is optically very thin so that $dz/d\tau'$ is large.

To check this prediction, the calculation leading to Fig. 1b was repeated but with the effects of CO_2 suppressed by setting all CO_2 transmittances to unity. Figure 2a shows the difference in tropopause height between this new, no-CO_2 calculation and the original calculation. The differences are less than 1 km over the parameter range of most practical interest, confirming that the effect of the 15-μm CO_2 band on the radiative constraint is indeed quite small. Interestingly, there are differences of both signs: CO_2 tends to lower the tropopause slightly when it is already low but raise it slightly when it is already high.

Now consider the effect of the 9.6-μm O_3 band, which happens to lie within the window region. Although this band is optically thick in the stratosphere, where O_3 concentrations are high, it is optically thin in the troposphere up to the tropopause. Thus, despite the high effective emission temperature of the upwelling radiation in this band, and despite the possibility of significant downwelling radiation emitted by stratospheric O_3, there is little absorption of radiation in this band near the tropopause. (In fact, when we calculated downwelling irradiances at the tropopause using the broadband model with and without O_3 we found differences of order 5 W m^{-2} or less, implying that the downwelling irradiance emitted by stratospheric O_3 is small too.) Hence, radiation in this band too is expected to have a small direct effect on tropopause temperature.

The calculation leading to Fig. 1b was also repeated with the effects of O_3 suppressed by setting all O_3 transmittances to unity. Figure 2b shows the difference in tropopause height between the no-O_3 calculation and the original calculation. The difference is strongly correlated with the tropopause height itself. For example,

where the original tropopause height is less than 14 km the difference is less than 2 km, but the difference rapidly increases as the original tropopause height increases. This behavior occurs because the calculations used a fixed O_3 profile with concentrations increasing rapidly above about 14 km. Thus, the argument in the previous paragraph is valid when H is lower than about 14 km but not when it is higher. The differences in Fig. 2b are positive for all parameter values, indicating that the IR effect of O_3 is to warm and lower the tropopause by absorbing some of the upwelling radiation in the window region. We shall see in the next section that the absorption of solar radiation by O_3 also tends to lower the tropopause.

Finally we consider the effects of the spectral variation in the radiative properties of water vapor. The calculation leading to Fig. 1b was repeated one more time with the effects of both CO_2 and O_3 suppressed, that is, retaining only the IR effects of water vapor. In the parameter range $T_* \approx 260$–300 K, $\gamma \approx 5$–7 K km^{-1} this H_2O-only calculation gives $H_{\rm RAD}$ some 2.5–5.0 km higher than the full broadband IR calculation (Fig. 2c), which in turn gives $H_{\rm RAD}$ 2–3 km higher than the minimal model shown in Fig. 1a. Also, this H_2O-only calculation retains the strong sensitivity of $H_{\rm RAD}$ to T_* throughout the $T_* - \gamma$ parameter space shown by the full broadband IR calculation. Thus there are two significant differences between the results of this broadband H_2O-only calculation and the minimal model gray atmosphere calculation: $H_{\rm RAD}$ is considerably higher, and the strong sensitivity of $H_{\rm RAD}$ to T_* is retained even for cold surface temperatures and steep lapse rates.

By tuning the relative humidity it is possible to reduce the difference in $H_{\rm RAD}$ between the broadband H_2O-only calculation and the minimal model calculation, but only slightly. For example, reducing the relative humidity from 50% to 30% in the broadband calculation lowers $H_{\rm RAD}$ by less than 1 km, while the minimal model $H_{\rm RAD}$ can be brought into line with the broadband H_2O-only calculation only by increasing the factor 0.2 in (5) by more than an order of magnitude—an implausibly large increase. It is therefore reasonable to attribute most of the differences between the broadband H_2O-only calculation and the minimal model gray atmosphere calculation to spectral variation in the radiative properties of water vapor.

In summary, spectral variations in the radiative properties of water vapor have a significant impact on the calculation of $H_{\rm RAD}$. For a fixed O_3 profile the IR effects of O_3 have a small impact for small $H_{\rm RAD}$ but an increasing impact as $H_{\rm RAD}$ increases. A different result would be expected if the O_3 profile were allowed to depend interactively on tropopause height. There is some compensation between these factors, with water vapor spectral variations tending to raise the tropopause, relative to a gray atmosphere calculation, while O_3 effects tend to lower the tropopause. The effects of CO_2 have a relatively small impact on the calculation of $H_{\rm RAD}$.

4. Sensitivity to solar heating and dynamical warming near the tropopause

In this section we assess the importance of non-IR warming such as solar heating and dynamical warming near the tropopause in determining the tropopause height. This is done by extending the simple radiative constraint model of section 2 to take account of non-IR warming. In each column the non-IR warming is assumed to be a specified function of height. The stratosphere is then defined to be that region in which net IR heating balances the specified non-IR warming, while the troposphere, as before, has a specified lapse rate.

As with the simpler version of the radiative constraint, there is a qualitative change in the heat budget between the troposphere and the stratosphere. In the troposphere, the lapse rate is thought to be determined by the combined effects of IR heating and convective and eddy heat transport, though a simple model for how this works is still lacking, and all of these processes may respond to changes in forcing parameters such as surface temperature. In the stratosphere, by constrast, the non-IR warming is determined by dynamical warming associated with the wave-driven mean meridional circulation and by absorption of solar radiation by O_3, which we consider to be fixed to a first approximation, while the tropopause height, stratospheric temperature, and net IR heating respond so as to achieve equilibrium.

Let the non-IR warming rate in W m^{-3} be $Q = \rho C_p \dot{T}_{\text{non-IR}}$, where ρ is the air density and C_p is the specific heat capacity at constant pressure. With the simple radiation model of section 2, the assumption that net IR heating balances non-IR warming in the stratosphere implies

$$Q = \frac{d}{dz}(U - D) \tag{10}$$

there. The problem, as before, is to find the lowest level $z = H_{\rm RAD}$ at which this balance is possible, for given T_* and γ. In fact $H_{\rm RAD}$ can be found without resorting to the optically thin stratosphere approximation by numerically evaluating certain integrals of the non-IR warming. Here, for simplicity, we will assume, as in our minimal radiative constraint model, that the stratosphere is optically thin. Then, substituting into (10) from (1) and (2) and neglecting the absorption of downwelling irradiance gives

$$B \approx \frac{1}{2}U - \frac{1}{3}Q\frac{dz}{d\tau} \tag{11}$$

at the tropopause. Since U is determined by the specified conditions in the lower troposphere and Q is specified, (11) determines B at the tropopause, and hence $T_{\rm TP} = (B/\sigma)^{1/4}$, and hence $H_{\rm RAD}$ through (3). Note, however,

that these equations determine H_{RAD} implicitly, because Q and τ are functions of z.

The ratio of the two terms on the right-hand side of (11) gives a dimensionless parameter

$$R = -Q \Big/ \left(\frac{3}{2} U \frac{d\tau}{dz}\right). \tag{12}$$

Physically R is the ratio of non-IR warming to heating by absorption of upwelling IR radiation. The magnitude of R measures the relative importance of non-IR warming, while its sign indicates whether non-IR warming is tending to warm the tropopause (positive R) or cool it (negative R). For example, using $\dot{T}_{\text{non-IR}} = 0.5$ K day^{-1} as a typical dynamical warming rate and taking $\rho = 0.12$ kg m^{-3}, $C_p \approx 10^3$ J kg^{-1} K^{-1}, $d\tau/dz = -10^{-5}$ m^{-1}, and $U = 200$ W m^{-2} gives a typical value for R of 0.23, implying that dynamical warming is of secondary importance but certainly not negligible. If, instead, we use a typical tropopause solar heating rate $\dot{T}_{\text{non-IR}} = 0.1$ K day^{-1}, then we find $R \approx 0.05$, implying that solar heating is rather less important.

We can use (11) to estimate the sensitivity of tropopause height to changes in the non-IR warming:

$$\frac{\partial H_{\mathrm{RAD}}}{\partial \dot{T}_{\text{non-IR}}} = \frac{\partial H_{\mathrm{RAD}}}{\partial T_{\mathrm{TP}}} \frac{\partial T_{\mathrm{TP}}}{\partial B_{\mathrm{TP}}} \frac{\partial B_{\mathrm{TP}}}{\partial \dot{T}_{\text{non-IR}}} \approx \left(\frac{1}{12} \frac{\rho C_p T}{\gamma B} \frac{dz}{d\tau}\right)\Bigg|_{\mathrm{TP}}. \tag{13}$$

For example, taking the values $T_{\mathrm{TP}} = 210$K, $\gamma = 6.5 \times 10^{-3}$ K m^{-1}, $B = 110$ W m^{-2}, and other parameters as above gives $\partial H_{\mathrm{RAD}}/\partial \dot{T}_{\text{non-IR}} \approx -3.1$ km (K day^{-1})$^{-1}$. In other words, 1 K day^{-1} of non-IR warming at the tropopause could lower the tropopause height by several kilometers.

There are considerable uncertainties in this estimate. The largest uncertainty is associated with uncertainty in the value of $dz/d\tau$ at the tropopause. (Note, by the way, that in our minimal model, where $\dot{T}_{\text{non-IR}}$ is neglected, H_{RAD} does not depend on $dz/d\tau$ at the tropopause.) The value of $dz/d\tau$ used here is based on the expression (4), taking $T_* \approx 270$ K and $z \approx 9$ km. However, the value of $dz/d\tau$ implied by (4) varies strongly with both T_* and z. Furthermore, the observed water vapor mixing ratio profile departs from the exponential form implied by (4), particularly in the upper troposphere and lower stratosphere. And, in addition, the optical properties of water vapor differ from those of an ideal gray atmosphere. Therefore, this estimate of the sensitivity of H_{RAD} to non-IR warming should be considered at best an order of magnitude estimate. Nevertheless, we have found sensitivities comparable to this estimate using a broadband radiative transfer model, discussed below, and in GCM experiments, discussed in the next section.

For a nongray atmosphere, an estimate for an effective, spectrally averaged $dz/d\tau$ at the tropopause can be obtained by using the broadband radiative transfer model to calculate the net upward irradiance U and its vertical gradient at the tropopause. Then, from (1),

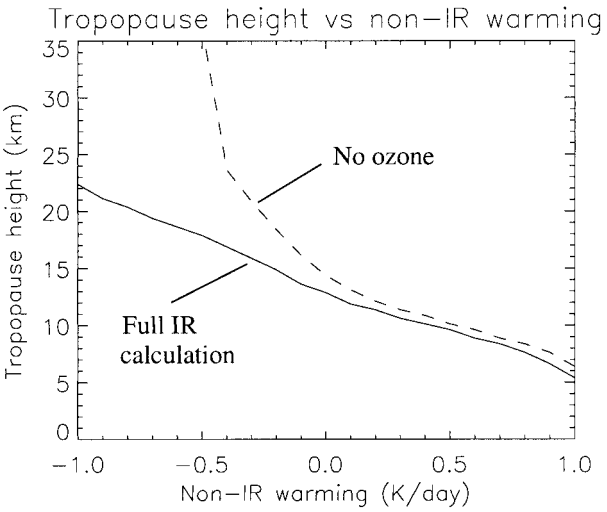

FIG. 3. Solid curve: tropopause height as a function of non-IR warming predicted by the broadband radiative–convective model. Dashed curve: the same, but with the IR effects of O_3 suppressed.

$$\frac{dz}{d\tau} = \frac{3}{2}(U - B) \Big/ \frac{dU}{dz}. \tag{14}$$

For a selection of typical temperature profiles this method gave tropopause values of $dz/d\tau$ in the range -0.5×10^5 to -10^5 m for the extratropics, with a larger value -4×10^5 m in the Tropics. Estimates made in a similar way using the net downward irradiance D gave a similar value in the Tropics but values roughly half as big in the extratropics. Again, these values suggest sensitivities of tropopause height to non-IR warming comparable to those given by the minimal model.

The sensitivity of tropopause height to non-IR warming can also be estimated directly using the broadband radiative–convective model. As before, the model was run with a CO_2 mixing ratio of 456 ppmv and a fixed O_3 profile typical of the Tropics. Surface temperature and lapse rate were set to $T_* = 280$ K and $\gamma = 6.5$ K km^{-1}, and the model was run to a steady state for a range of non-IR warming rates. The results are shown as the solid curve in Fig. 3. The curve is remarkably linear and gives a sensitivity of about 8 km (K day^{-1})$^{-1}$. A similar calculation using the minimal model (not shown) indicates a much more nonlinear response, with the sensitivity rapidly increasing as tropopause height increases and tropopause $dz/d\tau$ increases for more negative non-IR warming. In the full broadband model calculation this tendency is largely offset by the increasing importance of O_3 with increasing tropopause height. This is confirmed by the dashed curve in Fig. 3, which shows the results of a similar calculation but with all O_3 transmissivities set to unity.

5. GCM experiments

We have used a GCM to test the sensitivity of tropopause height to non-IR warming in the lower strato-

sphere predicted by the radiative constraint. The GCM used is the same version of the U.K. Universities Global Atmospheric Modelling Programme GCM used by Thuburn and Craig (1997). The most important details here are (i) the GCM was run at spectral T42 horizontal resolution, with 33 levels to give extra vertical resolution (roughly 0.5 km) near the tropopause; (ii) the model was run with fixed January solar and lower boundary forcing, in particular, the sea surface temperature (SST) and the temperature in the lowest layer of a shallow three-layer soil model were specified and fixed in time; and (iii) a specified climatological ozone distribution (Shine 1989) is used for the radiative heating calculations.

Five experiments were carried out. The first was a control experiment with the GCM in its standard configuration. The second and third experiments were designed to test the sensitivity to solar heating near the tropopause. In the second experiment the specified profile of ozone concentration was shifted downward by one pressure-scale height (approximately 7 km) while maintaining the same total column amount. In the third experiment the ozone was removed completely. These three experiments have already been discussed by Thuburn and Craig (1997). The experiments were run for 120 days and results are shown below for the last 30 days.

The fourth and fifth experiments were designed to test the sensitivity to dynamical warming near the tropopause. In the fourth experiment a zonally symmetric eastward force was imposed in the stratosphere with the distribution

$$f(p)(\sin 2\phi)^2 \times 5 \text{ m s}^{-1} \text{ day}^{-1}, \tag{15}$$

where

$$f(p) = \begin{cases} 1.0 & p < 10 \text{ hPa} \\ (100 \text{ hPa} - p)/90 \text{ hPa} & 10 \text{ hPa} < p < 100 \text{ hPa} \\ 0.0 & 100 \text{ hPa} < p. \end{cases} \tag{16}$$

This force is comparable in magnitude but opposite in sign to the force exerted on the real winter stratosphere by breaking and dissipation of quasi-stationary planetary waves, though its meridional extent is somewhat broader (e.g., Randel 1992). It therefore tends to drive a stratospheric residual mean meridional circulation in the opposite sense to the usual Brewer–Dobson circulation (e.g., Haynes et al. 1991), and so it weakens the tropical ascent and high-latitude descent. This in turn implies weaker dynamical cooling in the Tropics and weaker dynamical warming at high latitudes. The fifth experiment was the same as the fourth except that the sign of the imposed stratospheric force was reversed. This tends to enhance the Brewer–Dobson circulation, implying stronger dynamical cooling in the Tropics and stronger dynamical warming at high latitudes. Because of the long radiative timescale in the lower stratosphere, these experiments were run for 240 days to allow plenty of time for the model to adjust to the imposed forcing. In practice, model diagnostics from days 90 to 120 were found to be very similar to those from later in the integrations, so diagnostics from days 90 to 120 are shown for all five integrations.

Note that in the eastward-force and westward-force experiments the stratospheric winds are very different from those in the control experiment. As a result there are large differences in the resolved Eliassen–Palm flux convergence and in the parameterized gravity wave drag. Hence the difference between the eastward-force experiment and the control experiment in total driving of the residual mean meridional circulation is not given simply by (15) and (16), and the response is not a linear function of the forcing.

Figure 4 shows the zonal mean 30-day mean temperature from the five experiments. The control experiment (Fig. 4a) has a realistic temperature structure. Temperature decreases rapidly with altitude up to the high-latitude tropopause at about 200–300 hPa and the tropical temperature minimum at about 80 hPa. Above these levels temperature is nearly constant or increases with altitude in the stratosphere. In the shifted-ozone experiment (Fig. 4b) the tropical temperature minimum is slightly warmer and at a slightly lower altitude than in the control experiment, while the middle stratosphere is about 10 K cooler. In the no-ozone experiment (Fig. 4c) temperature decreases with altitude virtually everywhere, even in the stratosphere; nevertheless, there is a distinct change in static stability at about 200–300 hPa in the extratropics and at about 80 hPa in the Tropics, which can be identified as the tropopause.

In the eastward-force experiment (Fig. 4d), where the stratospheric meridional circulation is weakened, the tropical temperature minimum is warmer and at lower altitude than in the control experiment. The extratropical stratospheric temperature is also modified, with temperature minima occurring at a much higher altitude than in the control run: about 30 hPa over the North Pole and about 60 hPa at 60°S. In the westward-force experiment (Fig. 4e) the tropical temperature minimum is cooler and at a higher altitude than in the control experiment, while the extratropical lower stratosphere is warmer than in the control.

In order to test the predictions of the simple model discussed in section 4, we diagnosed the tropopause height for these five experiments and compared changes in tropopause height to changes in non-IR warming near the tropopause. Figure 5 shows the tropopause height for the five experiments, found column by column according to the World Meteorological Organization lapse rate definition then time averaged and zonally averaged. To begin with we focus on the extratropics, because there the tropopause as defined by the radiative constraint coincides quite closely with the tropopause defined by the lapse rate criterion, so we expect the ra-

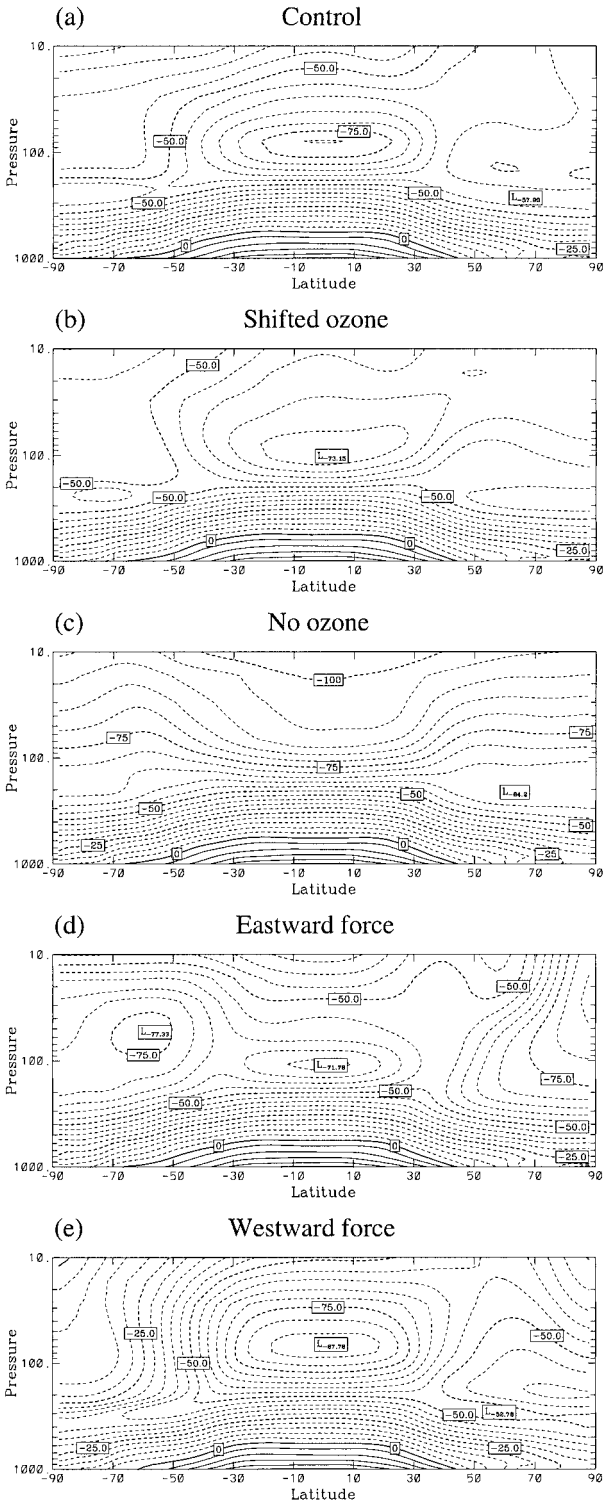

FIG. 4. Time mean, zonal mean temperature (°C) for the five GCM experiments: (a) control, (b) shifted ozone, (c) no ozone, (d) eastward stratospheric force, and (e) westward stratospheric force.

diative constraint to make useful predictions about its sensitivity to non-IR warming.

In the shifted-ozone experiment the extratropical tropopause height is within 0.5 km of that in the control experiment. Indeed, near the summer pole there is virtually no difference in tropopause height. The solar heating rate near the summer extratropical tropopause is roughly 0.15 K day^{-1} greater than that in the control experiment, implying a sensitivity $\partial H_{\mathrm{RAD}}/\partial \dot{T}_{\text{non-IR}}$ rather less than that estimated in section 4.

In the no-ozone experiment the extratropical tropopause height is 0.5–1 km higher than in the control experiment in the winter hemisphere and 1.5–2 km higher in the summer hemisphere. The solar heating rate near the summer extratropical tropopause in the control experiment is less than about 0.1 K day^{-1}, while in the no-ozone experiment it is virtually zero. If the solar heating were the only difference between this experiment and the control these results would imply a sensitivity $\partial H_{\mathrm{RAD}}/\partial \dot{T}_{\text{non-IR}}$ much greater than that estimated in section 4. However, it is likely that the IR effects of removing O_3 are also significant in raising the tropopause, becoming more so as H increases (see Fig. 3).

In the eastward-force experiment the extratropical tropopause is about 1.5–2 km higher than in the control experiment. At the winter pole the diagnosed tropopause appears up to 3 km higher, though it is not clear that a well-defined tropopause really exists there. The dynamical warming rate near the extratropical tropopause is reduced by about 0.4 K day^{-1} in both hemispheres, from about 0.4–0.5 K day^{-1} in the control experiment to nearly zero in the eastward-force experiment. These figures imply a sensitivity $\partial H_{\mathrm{RAD}}/\partial \dot{T}_{\text{non-IR}}$ close to that estimated in section 4.

In the westward-force experiment the extratropical tropopause is lower than in the control experiment, about 1.5–2 km lower in the summer hemisphere and about 1 km lower in the winter hemisphere. The dynamical warming rates near the tropopause are greater than in the control experiment by about 0.3 K day^{-1} in the summer and about 0.2 K day^{-1} in the winter. Again these figures imply a sensitivity $\partial H_{\mathrm{RAD}}/\partial \dot{T}_{\text{non-IR}}$ close to that estimated in section 4.

In the Tropics different definitions of the tropopause give significantly different tropopause heights (e.g., Highwood and Hoskins 1998). For our control experiment the lapse rate tropopause is typically found 1–2 km below the temperature minimum, while the top of the convectively adjusted region is typically found another 3 km lower still (Thuburn and Craig 1997). Therefore, in the Tropics, we should not expect the radiative constraint to accurately predict the height of the lapse rate tropopause or its sensitivity to non-IR warming. An interesting question is whether, in fact, the radiative constraint actually predicts the height and sensitivity of the top of the tropical convection. In a radiative–convective model the height of the top of convection is, by definition, H_{RAD}. In the real atmosphere the situation is rath-

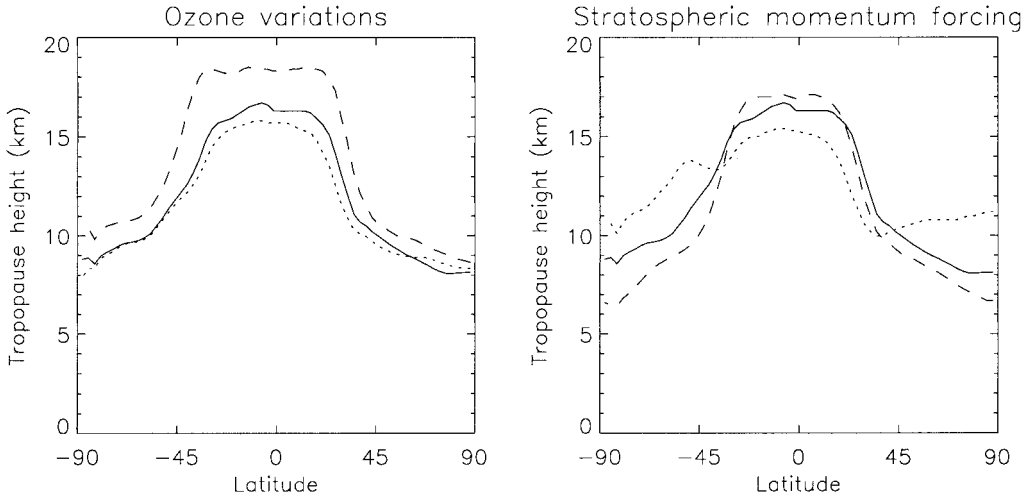

FIG. 5. Time mean, zonal mean tropopause height, diagnosed using the lapse rate criterion, for the five GCM experiments. (Left) Solid curve: control. Dotted curve: shifted ozone. Dashed curve: no ozone. (Right) Solid curve: control. Dotted curve: eastward stratospheric force. Dashed curve: westward stratospheric force.

er more complicated. There is a wide spectrum of cumulus top heights, with a few clouds reaching at least as high as the level of minimum temperature (e.g., Danielsen 1993) and many clouds overshooting their level of neutral buoyancy.

Our GCM results do at least show that the convection top height is influenced by the stratospheric meridional circulation. Figure 6 shows the zonal mean temperature tendency due to cumulus convection from the eastward-force, control, and westward-force experiments. There is a small but clear and systematic increase in the depth of the convective heating as the stratospheric residual mean meridional circulation increases in strength. [The negative cumulus heating rates at the very top of the convection are an artefact of the particular convective parameterization scheme used; see Thuburn and Craig (1997) for more details.] A similar trend is visible in other related diagnostics such as the height of the poleward branch of the Hadley circulation.

In summary, these GCM experiments show a sensitivity of extratropical tropopause height to non-IR warming of a few kilometers per K day^{-1}, with stronger (more positive) warming leading to a lower tropopause, though the magnitude of the sensitivity depends strongly on the process causing the warming and on the sign of the warming. Our simple model for the radiative constraint also predicts a sensitivity of a few kilometers per K day^{-1}, with the potential for large variations because

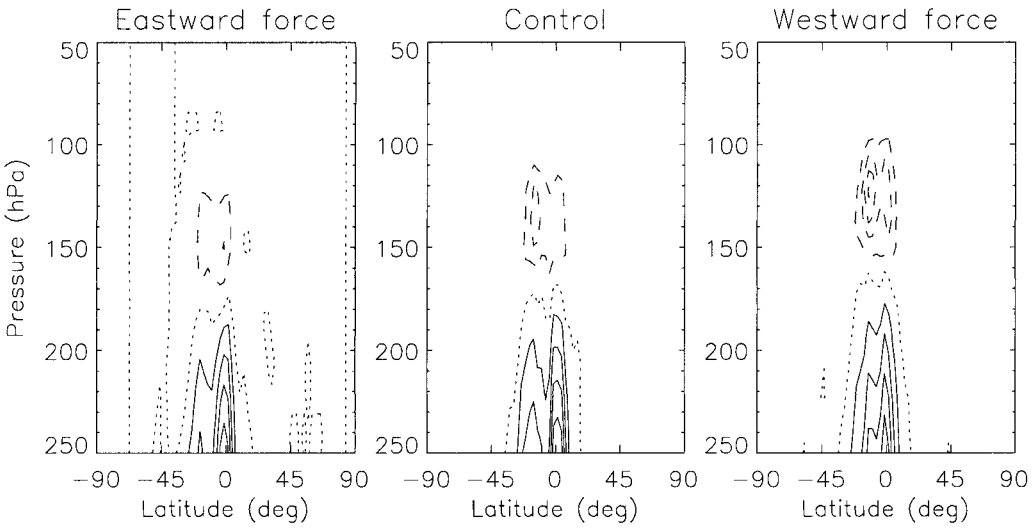

FIG. 6. Time mean, zonal mean cumulus heating for three GCM experiments. (Left) Eastward stratospheric force. (Center) Control. (Right) Westward stratospheric force. Contour interval 0.5 K day^{-1}, positive contours solid, zero contour dotted, negative contours dashed.

of the large variations in the $dz/d\tau$ term. In the Tropics, both the height of the temperature minimum and the height of the main convective outflow are sensitive to non-IR warming.

6. Summary and discussion

The concept of a radiative constraint on tropopause height has been reexamined. The essential physics underlying the radiative constraint is that the IR emission from the level of the tropopause, which depends on its temperature, must balance all the factors tending to warm the tropopause, including absorption of upwelling IR from the troposphere, solar heating, and dynamical warming. For a given surface temperature and tropospheric lapse rate, the tropopause temperature determines the tropopause height. A minimal quantitative model for the radiative constraint can be obtained using a two-stream gray atmosphere radiative model for IR radiatiation and neglecting solar heating, dynamical warming, and absorption of IR radiation downwelling from the stratosphere.

We have investigated the importance of some of the factors neglected in our minimal model of the radiative constraint—namely, the spectral dependence of the radiative properties of the atmosphere in the IR, and non-IR warming near the tropopause. For the first of these factors we have compared the predictions of our minimal model with those of a more complete model based on the Morcrette (1990) broadband radiation scheme. The tropopause heights predicted by the two models differ by 2–3 km. This difference appears to be accounted for mainly by spectral variations in the radiative properties of water vapor, with O_3 effects partly compensating. The sensitivity of tropopause height to surface temperature and tropospheric lapse rate predicted by the two models is mostly very similar. An exception occurs for very cold surface temperatures and steep lapse rates where the minimal model achieves an optically thin limit with weaker sensitivity to surface temperature, whereas the broadband model does not.

We have extended our minimal model to include the effects of specified non-IR warming near the tropopause. It predicts a sensitivity of a few kilometers per K day^{-1}, with positive non-IR warming leading to a warmer, lower tropopause. There is a large uncertainty in this estimate, however, because of the large uncertainty in $dz/d\tau$. A similar magnitude of sensitivity was found in a more sophisticated calculation based on the broadband radiation scheme. We investigated this sensitivity further by carrying out GCM experiments with imposed changes in solar heating or with imposed zonal forces in the stratosphere leading to modified dynamical warming near the tropopause. In the extratropics, where we believe the radiative constraint to be most applicable, we found sensitivities of the order of a few kilometers per K day^{-1}, though with large variations.

The height of the observed extratropical tropopause has a distinct seasonal cycle, with interesting asymmetries between the hemispheres (Appenzeller et al. 1996). The stratospheric meridional circulation also has a distinct seasonal cycle, again with some asymmetries between the hemispheres (Rosenlof 1995). The radiative constraint, and the sensitivity it predicts to non-IR warming, should enable us to begin to make a quantitative link between these two.

In the Tropics, the radiative constraint is not expected to be a useful model for the height of the temperature minimum, though it may be a useful model for the height of the main convective outflow level. In the GCM experiments the height of the tropical temperature minimum showed considerable sensitivity to both dynamical warming and ozone heating. In the extreme case where ozone heating was removed completely tropical temperatures decreased with altitude up to the model top near 10 hPa. The sensitivity of the height and temperature of the tropical temperature minimum to dynamical warming associated with the stratospheric meridional circulation is consistent with the results of Yulaeva et al. (1994) and Mote et al. (1996). An interesting question is, how far down below the temperature minimum does the influence of the stratospheric circulation extend? Zhang (1993) presents evidence for a seasonal cycle in tropical cirrus cloud cover above about 15 km whose phase is consistent with that of the stratospheric circulation. Our GCM results show that the influence of the stratospheric circulation extends down at least as far as the main convective outflow level near 12–13 km, some 5 km below the January temperature minimum.

It is sometimes remarked that the slope of the extratropical tropopause resembles the slope of tracer isolines in the lowermost stratosphere, and that perhaps there might be some link between the two. It is true that the stratospheric meridional circulation tends to tilt both the tropopause and tracer isolines in the same sense. However, the mechanisms are rather different. For long-lived tracers, the slope results from a competition between advection by the mean meridional circulation and quasi-horizontal mixing (e.g., Mahlman et al. 1986). In the case of the tropopause, the tropopause temperature results from a competition between dynamical warming (vertical advection of potential temperature) and IR radiation; the actual slope then depends on latitudinal variations in dynamical warming, upwelling IR radiation, and tropospheric temperature profile. In particular, we would expect the tropopause to slope even if there were no stratospheric mean meridional circulation. This is confirmed by our eastward-force experiment, which shows the tropopause sloping in the usual upward-equatorward sense even though the stratospheric circulation is extremely weak in both hemispheres and actually reversed in the Southern Hemisphere.

Finally, a possible application of our results may be to help understand systematic errors in GCMs. A widespread problem among GCMs is a systematic cold bias of the extratropical tropopause and lowermost strato-

sphere (Boer et al. 1992). Johnson (1997) discusses this cold bias in terms of a spurious numerical source of entropy that must be present in most GCMs. The use of a semi-Lagrangian advection scheme helps to reduce the cold bias (Chen and Bates 1996). M. Blackburn (1997, personal communication) has shown that in an Eulerian spectral model errors in the advection of water vapor leading to errors in radiative heating are responsible for the initial cooling, but this does not explain the long term maintenance of the cold bias. The cold bias is also reduced in GCMs with a hybrid isentropic vertical coordinate (Zhu and Schneider 1997; Webster et al. 1999). A possible explanation, consistent with our results presented here, is that some aspect of the dynamics, such as propagation or breaking of planetary waves, is more accurately represented in semi-Lagrangian and hybrid isentropic coordinate models than in traditional Eulerian pressure-based coordinate models, leading to stronger descent and dynamical warming and hence a warmer, lower tropopause at high latitudes.

Acknowledgments. The GCM experiments reported here were carried out under the U.K. Universities Global Atmospheric Modelling Programme, funded by the U.K. Natural Environment Research Council.

REFERENCES

Appenzeller, C., J. R. Holton, and K. H. Rosenlof, 1996: Seasonal variation of mass transport across the tropopause. *J. Geophys. Res.,* **101,** 15 071–15 078.

Bethan, S., G. Vaughan, and S. J. Reid, 1996: A comparison of ozone and thermal tropopause heights and the impact of tropopause definition on quantifying the ozone content of the troposphere. *Quart. J. Roy. Meteor. Soc.,* **122,** 929–944.

Boer, G. J., and Coauthors, 1992: Some results from an intercomparison of the climates simulated by 14 atmospheric general circulation models. *J. Geophys. Res.,* **97,** 12 771–12 786.

Chen, M. H., and J. R. Bates, 1996: A comparison of climate simulations from a semi-Lagrangian and an Eulerian GCM. *J. Climate,* **9,** 1126–1148.

Danielsen, E. F., 1993: In situ evidence of rapid, vertical, irreversible transport of lower tropospheric air into the lower tropical stratosphere by convective cloud turrets and by larger-scale upwelling in tropical cyclones. *J. Geophys. Res.,* **98,** 8665–8681.

Forster, P. M. de F., R. S. Freckleton, and K. P. Shine, 1997: On aspects of the concept of radiative forcing. *Climate Dyn.,* **13,** 547–560.

Goody, R. M., 1964: *Atmospheric Radiation, I: Theoretical Basis.* Clarendon Press, 436 pp.

Haynes, P. H., C. J. Marks, M. E. McIntyre, T. G. Shepherd, and K. P. Shine, 1991: On the ''downward control'' of extratropical diabatic circulations by eddy-induced mean zonal forces. *J. Atmos. Sci.,* **48,** 651–678.

Held, I. M., 1982: On the height of the tropopause and the static stability of the troposphere. *J. Atmos. Sci.,* **39,** 412–417.

Highwood, E. J., and B. J. Hoskins, 1998: The tropical tropopause. *Quart. J. Roy. Meteor. Soc.,* **124,** 1579–1604.

Hoerling, M. P., T. K. Shaack, and A. J. Lenzen, 1991: Global objective tropopause analysis. *Mon. Wea. Rev.,* **119,** 1816–1831.

IPCC, 1994: Radiative forcing. *Climate change (1994) Radiative forcing of climate change and an evaluation of IPCC IS92 emission scenarios,* J. T. Houghton, et al., Eds., Cambridge University Press, 163–199.

Johnson, D. R., 1997: ''General coldness of climate models'' and the second law: Implications for modeling the Earth system. *J. Climate,* **10,** 2826–2846.

Lewis, R. P. W., Ed., 1991: *Meteorological Glossary*. 6th ed., HMSO, 335 pp.

Lowe, P. R., 1977: An approximating polynomial for the computation of saturation vapor pressure. *J. Appl. Meteor.,* **16,** 100–103.

Mahlman, J. D., H. Levy II, and W. J. Moxim, 1986: Three-dimensional simulations of stratospheric N_2O: Predictions for other trace constituents. *J. Geophys. Res.,* **91,** 2687–2707.

Morcrette, J.-J., 1990: Impact of changes to the radiation transfer parametrizations plus cloud optical properties in the ECMWF model. *Mon. Wea. Rev.,* **118,** 847–873.

Mote, P. W., and Coauthors, 1996: An atmospheric tape recorder: The imprint of tropical tropopause temperatures on stratospheric water vapor. *J. Geophys. Res.,* **101,** 3989–4006.

Randel, W. J., 1992: Global atmospheric circulation statistics, 1000-1mb. NCAR Tech. Note NCAR/TN-366+STR, 256 pp. [Available from National Center for Atmospheric Research, P.O. Box 3000 Boulder, CO 80307-3000.]

Rosenlof, K. H., 1995: Seasonal cycle of the residual mean meridional circulation in the stratosphere. *J. Geophys. Res.,* **100,** 5173–5191.

Shine, K. P., 1989: Sources and sinks of zonal momentum in the middle atmosphere diagnosed using the diabatic circulation. *Quart. J. Roy. Meteor. Soc.,* **115,** 265–292.

Sinha, A., and K. P. Shine, 1994: A one-dimensional study of possible cirrus cloud feedbacks. *J. Climate,* **7,** 158–173.

Thuburn, J., and G. C. Craig, 1997: GCM tests of theories for the height of the tropopause. *J. Atmos. Sci.,* **54,** 869–882.

Webster, S., J. Thuburn, B. J. Hoskins, and M. Rodwell, 1999: Further development of a hybrid-isentropic GCM. *Quart. J. Roy. Meteor. Soc.,* **125,** 2305–2331.

Yulaeva, E., J. R. Holton, and J. M. Wallace, 1994: On the cause of the annual cycle in the lower tropical stratospheric temperature. *J. Atmos. Sci.,* **51,** 169–174.

Zhang, C., 1993: On the annual cycle in highest, coldest clouds in the Tropics. *J. Climate,* **6,** 1987–1990.

Zhong, W., and J. D. Haigh, 1995: Improved broadband emissivity parameterization for water vapor cooling rate calculations. *J. Atmos. Sci.,* **52,** 124–138.

——, R. Toumi, and J. D. Haigh, 1996: Climate forcing by stratospheric ozone depletion calculated from observed temperature trends. *Geophys. Res. Lett.,* **23,** 3183–3186.

Zhu, Z., and E. K. Schneider, 1997: Improvement in stratosphere simulation with a hybrid $\sigma - \theta$ coordinate GCM. *Quart. J. Roy. Meteor. Soc.,* **123,** 2095–2113.